Article

Tracing Water–Rock–Gas Reactions in Shallow Productive Mud Chambers of Active Mud Volcanoes in the Caspian Sea Region (Azerbaijan)

Aygun Bayramova [1], Orhan R. Abbasov [1], Adil A. Aliyev [1], Elnur E. Baloglanov [1], Franziska M. Stamm [2], Martin Dietzel [2] and Andre Baldermann [2,*]

1   Mud Volcanism Department, Institute of Geology and Geophysics, Ministry of Science and Education of the Republic of Azerbaijan, H. Javid Av., 119, Baku AZ1143, Azerbaijan; bayramova.aygun97@gmail.com (A.B.); ortal80@bk.ru (O.R.A.); ad_aliyev@mail.ru (A.A.A.); elnur1001@mail.ru (E.E.B.)
2   Institute of Applied Geosciences & NAWI Graz Geocenter, Graz University of Technology, Rechbauerstraße 12, 8010 Graz, Austria; fstamm@tugraz.at (F.M.S.); martin.dietzel@tugraz.at (M.D.)
*   Correspondence: baldermann@tugraz.at; Tel.: +43-(0)316-873-6850

Abstract: We present geochemical and mineralogical datasets for five new mud volcanoes in continental Azerbaijan (Hamamdagh and Bendovan) and the adjacent Caspian Sea (Khara-Zire, Garasu and Sangi-Mughan). The fluid ejects have a Na–Cl-type composition and are generated by the mixing of evaporated Caspian seawater and low- to high-salinity pore waters, as indicated by Br–B and Cl–B systematics and Na–K and SiO_2 geo-thermometers. The fluids contain high concentrations of As, Ba, Cu, Si, Li, Sr and Zn (60 to 26,300 ppm), which are caused by surface evaporation, pyrite oxidation, ion exchange reactions and hydrocarbon maturation in Oligocene-Miocene 'Maykop' shales. The solid ejects comprise liquid, oily and brecciated mud, mud/claystones and sandstones. The mud heterogeneity of the volcanoes is related to the geological age and different sedimentological strata of the host rocks that the mud volcanoes pass through during their ascent. All ejects show evidence of chemical alterations via water–rock–gas reactions, such as feldspar weathering, smectite illitization and the precipitation of Fe-(hydr)oxides, calcite, calcian dolomite, kaolinite and smectite. The studied localities have petrographic similarities to northern extending mud volcano systems located on Bahar and Zenbil islands, which suggests that mud volcanoes in the Caspian Sea region are sourced from giant shallow mud chambers (~1–4 km depth) located in Productive Series strata. Our results document the complex architecture of the South Caspian Basin—the most prolific hydrocarbon region in the world.

Keywords: mud volcanism; seep water chemistry; water-rock interaction; mud mineralogy; mud chemistry; Caspian Sea; Azerbaijan; Productive Series; Maykop shales

1. Introduction

Mud volcanoes provide a unique window to the architecture of sedimentary basins, convergent margins and subduction zones [1,2]. They produce scenic landscapes and morphological features on the Earth's surface, such as gryphons, mud and scoria cones, salses, springs and fire columns [3–6]. However, the release of toxic and radioactive elements (arsenic, As; barium, Ba; copper, Cu; strontium, Sr; uranium, U; zinc, Zn, etc.) and (a) biogenic gases (e.g., methane, CH_4 and minor carbon dioxide, CO_2) during the active and dormant periods of volcanoes can impact the chemistry of local surface water, groundwater, interstitial solutions and sediments, as well as the Earth's atmospheric gas budget [7–16]. In many places, mud volcanic activity is triggered by the rapid subsidence of soft, fine-grained sediments rich in water and organic matter in a compressive tectonic setting, which promotes the generation of hydrocarbons and, subsequently, the formation

of fluid–mud–gas mixtures migrating upward along fractures and faults in the compacted host rocks under overpressure [1,17,18].

Mud volcanoes are pervasive within the Caspian Sea region, particularly in Azerbaijan, which is a transcontinental country located at the boundary between Eastern Europe and Western Asia (Figure 1a). Thus far, 353 mud volcanoes have been identified in East Azerbaijan and in the shallow-water area of the South Caspian Sea, both onshore (199) and offshore (154) [3,19–21]. Mud volcanism in this area was caused by (i) fast sedimentation rates of up to 2.4 km per million years in the Pliocene, (ii) massive CH_4 production in the Miocene–Pliocene 'Productive Series' sediments and in the Oligocene–Miocene 'Maykop' shales, (iii) the presence of major folding zones and (iv) the tectonic compression of the South Caspian Basin [14,22,23]. The latter causes the generation of low-density fluid–mud–gas mixes from ~1 to 8 km in depth [5], which migrate upward in the compacted, fractured sedimentary rocks [1]. The resulting mud diapirism ejects clay-rich sediments that form the Earth's landscape, in addition to escaping fluid and gas phases [5,7,13,15,24]. However, the age of the basement, the beginning and progression of mud diapirism and the origin of the South Caspian Basin are disputed, with most published models postulating an initiation between the Jurassic and Miocene [25].
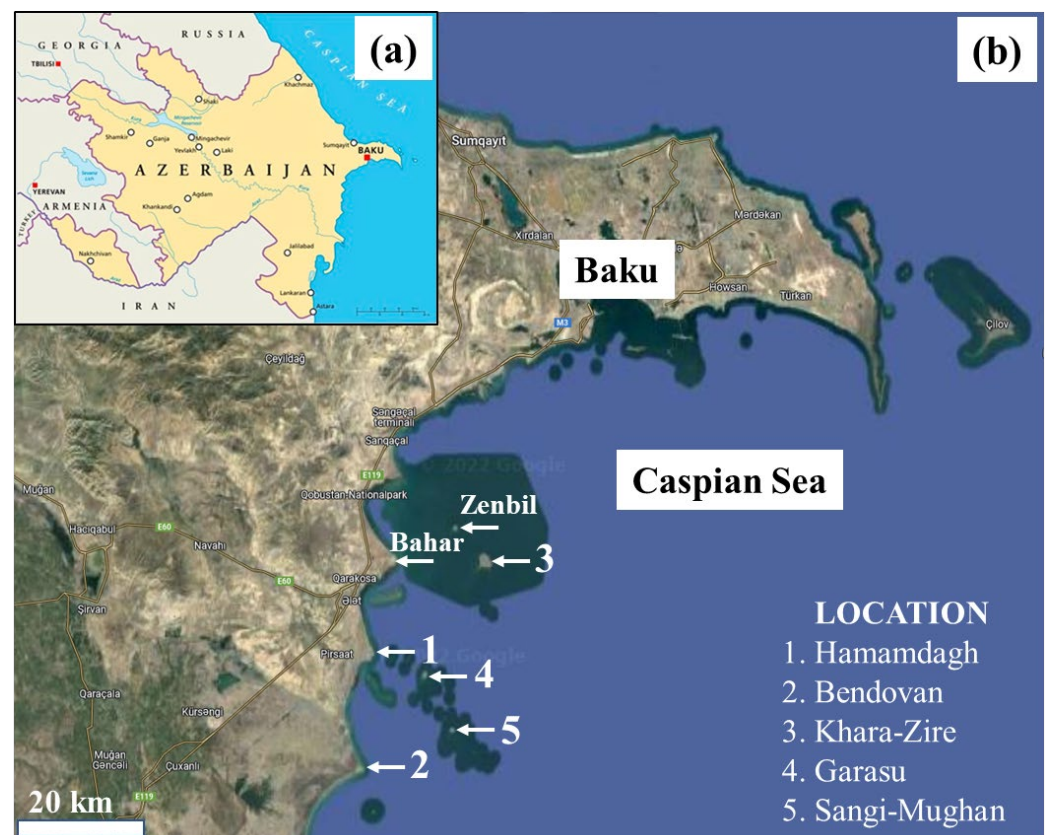

Figure 1. (**a**) Location map of Azerbaijan in Western Asia. (**b**) Google Earth view showing the location of the investigated mud volcanoes in the Baku area (onshore sites: 1 and 2) and on islands within the Caspian Sea (offshore sites: 3–5), Azerbaijan.

The widespread, active and passive mud volcano systems located onshore in East Azerbaijan are relatively well documented with respect to their fluid and solid ejects [4,11,26–28]. On the contrary, ejects of island mud volcanoes are much less well characterized. This is because conventional sampling is difficult due to the isolated location of these islands in the Caspian Sea. For instance, more than eight new islands formed within the Baku archipelago and the Caspian Sea region as a result of (sub)recent mud volcanic eruptions, but these sites remain unexplored (Khara-Zire, Garasu, Gil and Sangi-Mughan). To the best

of our knowledge, only Baldermann et al. [16] have reported on the mineralogical, textural and chemical compositions of fluid and mud ejects from Zenbil island, which is located in the coastal water of the Caspian Sea. The authors compare the mud mineralogy from Zenbil with onshore material collected from the mud volcano system at Bahar, concluding that the mud has a homogenous composition at the two localities, thus originating from the same shallow-seated mud chamber. In this study, the mineralogical and geochemical compositions of expelled mud, sedimentary rocks and seep water from five prominent mud volcanoes were studied for the first time. The origin of the fluids and the provenance of the mud are discussed.

2. Materials and Methods

2.1. Materials

The study sites, Hamamdagh and Bendovan, are located in the Salyan region, ~60 km and ~80 km southwest of Baku (Azerbaijan), respectively, and are similar to the onshore mud volcano system at Bahar (Figure 1b, locations 1–2). The sites Khara-Zire, Garasu and Sangi-Mughan are located in the Caspian Sea, ~40 km, ~60 km and ~70 km southwest of Baku, respectively, and are similar to the offshore mud volcano system at Zenbil (Figure 1b, locations 3–5). Thus, the new mud volcanoes studied here are located in a southern direction from the mud volcanoes of Zenbil and Bahar.

Solid and fluid samples were taken from all mud volcanoes during a field campaign carried out in October 2021 (Figure 2). Mud suspensions were collected from gryphon-type emissions within the central mud crater at each study site. The fresh mud suspensions appear as fine-grained sediments of a grey color dispersed in a liquid that is dominated either by water or a water–oil mixture, henceforth called liquid mud and oily mud, respectively (cf. Figure 2a,b). The oily mud contains liquid hydrocarbons and has an oily appearance and a strong smell of hydrogen sulfide. Some mud emissions are mixed with CH_4 gas (indicated by bubbling); however, the gas phase was not sampled in this study. In total, 33 solid samples were taken from the different study sites, which include liquid mud suspensions (6 samples, Figure 2a,d,f), oily mud suspensions (5 samples, Figure 2b), as well as 3 types of partly consolidated or fully consolidated sedimentary rocks, light grey to dark grey in color. The latter appear as (i) 'brecciated' mud crusts with desiccation cracks (4 samples, Figures 2e and 3a), (ii) claystones (9 samples, Figures 2c and 3b) and (iii) sandstones (6 samples, Figure 3c). All sample types occasionally contain euhedral pyrite crystals ranging from millimeters to centimeters in size, which were isolated via hand picking (3 samples).

Solid and fluid samples were prepared in the laboratories of the Institute of Geology and Geophysics, Ministry of Science and Education of the Republic of Azerbaijan, and the Institute of Applied Geosciences, Graz University of Technology. The fluids were filtered through 0.45 μm cellulose acetate membrane filters (Sartorius, Vienna, Austria) and separated in three aliquots for subsequent measurements of (i) temperature, alkalinity, pH and electric conductivity (EC), (ii) major cations and anions and (iii) dissolved trace elements. For the trace elemental analysis, the fluid samples were acidified to a 2% nitric acid (HNO_3) matrix using HNO_3 of suprapure grade (Roth, ROTIPURAN®, Karlsruhe, Germany). The solids were dried at 40 °C and subsequently ground using an agate mortar and pestle.
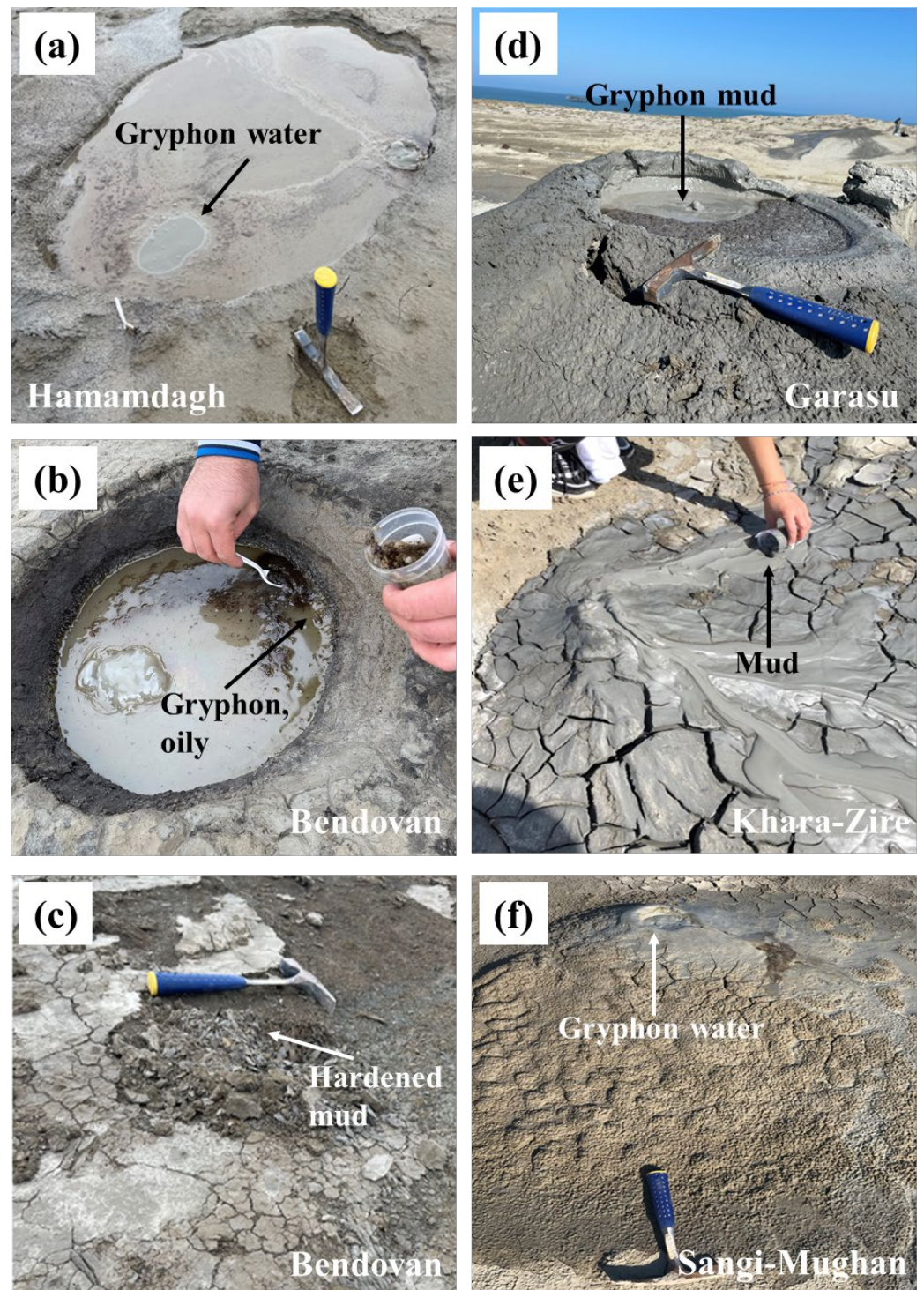
Figure 2. Photographs showing field impressions and specific sampling sites at the mud volcanoes in (**a**) Hamamdagh, (**b**,**c**) Bendovan, (**d**) Garasu, (**e**) Khara-Zire and (**f**) Sangi-Mughan, located in the Baku area and on islands within the Caspian Sea, Azerbaijan.
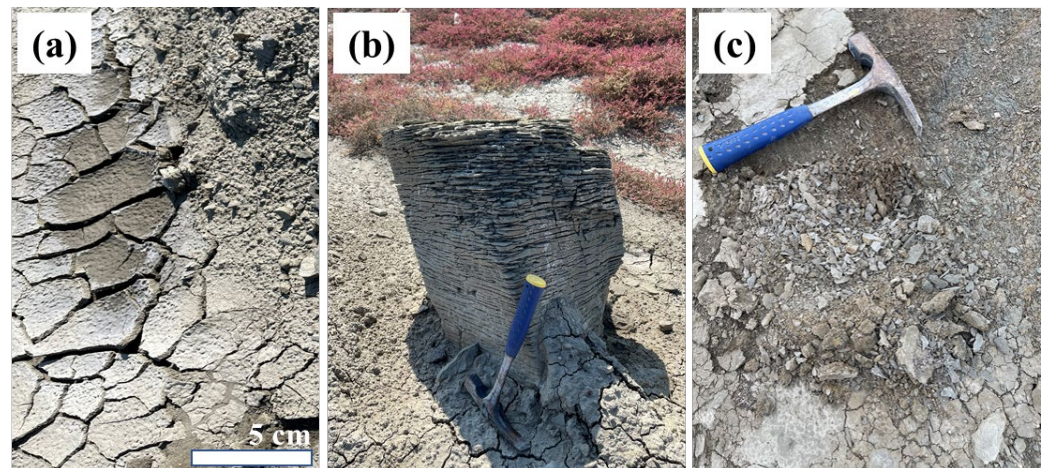
Figure 3. Photographs showing mud and sedimentary rock ejects from the mud volcano at Khara-Zire, offshore in the Caspian Sea, Azerbaijan. (**a**) Brecciated mud with desiccation cracks. (**b**) Claystone. (**c**) Sandstone fragments.

2.2. Analytical Methods

2.2.1. Fluid Phase Characterization

A SenTix 41 glass electrode connected to a WTW Multi 350i pH meter was used to determine the pH and temperature of the extracted fluids. The pH electrode was calibrated using NIST standard buffer solutions at pH 7.00 and 10.00 at 25 °C. The analytical error was ±0.03 pH units. For the determination of the EC values, a WTW LF 330 m connected to a WTW Multi 350i probe was used (analytical error: <3%; WTW GmbH, Weilheim, Germany). Total alkalinity was determined via the automated titration of a 0.1 M hydrochloric acid (HCl) solution using a Schott TitroLine alpha plus titrator (Xylem Analytics Germany Sales GmbH & Co. KG, Weilheim, Germany) with an analytical accuracy of ±2% [29].

A Dionex ICS-3000 ion chromatograph (Thermo Fisher Scientific Inc., Waltham, MA, USA) was used to analyze the concentrations of the major cations (sodium, Na^+, potassium, K^+, calcium, Ca^{2+} and magnesium, Mg^{2+}) and anions (chloride, Cl^-, sulphate, SO_4^{2-} and bromide, Br^-) in filtered, non-acidified samples with an analytical error of <3% [30]. The total dissolved trace element concentrations (silver, Ag; aluminum, Al; As; boron, B; Ba; cadmium, Cd; cobalt, Co; chromium, Cr; Cu; iron, Fe; lithium, Li; manganese, Mn; nickel, Ni; phosphorous, P; lead, Pb; silicon, Si; Sr; and Zn) were analyzed in acidified aliquots using a PerkinElmer Optima 8300 DV optical emission spectrometer with inductively coupled plasma (PerkinElmer, Waltham, MA, USA). The analytical precision was better than ±3% (2σ, 3 replicates), as determined by replicate analyses of NIST 1640a, as well as in-house and SPS-SW2 Batch 130 (Merck KGaA, Darmstadt, Germany) standards [31].

The PHREEQC software (version 2.18.00) with its llnl.dat database was used to calculate the species distribution, activities, ionic strength, ionic charge balances and saturation indices (SI) of the fluids with respect to relevant mineral phases, such as feldspars, carbonates and clay minerals [32].

Fluid generation temperatures were calculated using common chemical geo-thermometers (Na-K, K-Mg, and SiO_2), which were originally designed for and applied to low- to high-salinity pore fluids generated in oil and gas basins [33–35]:

$$T_{Na/K} \ (^{\circ}C) = 1217/(1.48 + \log(Na/K)) - 273.15$$

$$T_{K/Mg} \ (^{\circ}C) = 4410/(14.0 - \log(K^2/Mg) - 273.15$$

$$T_{SiO2} \ (^{\circ}C) = 1522/(5.75 - \log(SiO_2)) - 273.15$$

A discussion of the applicability and limitations of these geo-thermometers is provided elsewhere [36].

2.2.2. Solid Phase Characterization

The quantitative mineralogical composition of the solids was determined using powder X-ray diffraction (P-XRD). The top loading method was applied to prepare the powdered materials in standard XRD sample holders [37], which were examined using a PANalytical X'Pert PRO diffractometer in a range from 4 to 85° 2θ with a step of 0.008° 2θ and a count time of 40 s per step. This device is equipped with a Scientific X'Celerator detector and a Co-Kα X-ray radiation source operating at 40 kV and 40 mA. Mineral identification was carried out using the PANalytical X'Pert Highscore Plus software (version 2.2e) and a pdf-4 database, based on the following criteria: quartz (peaks at 4.25 Å and 3.34 Å), calcite (peaks at 3.85 Å and 3.03 Å), dolomite (peak at ~2.9 Å for dolomite stoichiometry; intensity ratio of the $d_{(105)}/d_{(110)}$ peaks for dolomite ordering degree), albite (peak at 3.19 Å), orthoclase (peak at 3.24 Å), pyrite (peaks at 2.71 Å and 1.63 ÅÅ), chlorite (peaks at ~14.2 Å, 4.71 Å and 1.54 Å), kaolinite (peaks at 7.15 Å, 3.57 Å and 1.49 Å), illite (peaks at ~10 Å, 4.99 Å and 1.50 Å) and smectite (broad peaks at ~13.5 Å and 1.50 Å). Randomly oriented mounts (<2 μm size fraction) were prepared and X-rayed as indicated before, each in air-dried, glycolated and heated (550 °C for 1 h) states, to exclude mixed-layered phases in the samples. Subsequently, mineral quantification was carried out via Rietveld refinement of P-XRD patterns using the PANalytical X'Pert Highscore Plus software (version 2.2e) and its implemented ICSD database with an analytical error of <3 wt.%, judged by comparing with chemical data and interlaboratory, cross-method calibration [38].

The chemical composition of the solids was analyzed using an Epsilon 4 benchtop energy-dispersive X-ray fluorescence (XRF) spectrometer. Approximately 1.0 g of sample was heated to 950 °C for 1 h to remove volatiles. Then, the loss on ignition (LOI) was determined via standard gravimetric analysis. Glass tablets were produced via the fusion of 6.0 g of $Li_2B_4O_7$ (fluid agent) and 0.6 g of sample at ~1200 °C in a PANalytical Perl X 3 bead preparation system (Malvern Panalytical, Malvern, United Kingdom). To avoid volatilization and loss of sulfur, the fusion time was reduced to ~3 min. The glass tablets were measured together with a set of USGS standards. For the major elements (expressed as oxides), the analytical error was <0.5 wt.% [39].

The Chemical Index of Alteration (CIA) was calculated from these chemical data, according to the expression $(Al_2O_3/(Al_2O_3 + Na_2O + K_2O + CaO^*)) \cdot 100$ [40], to quantitatively determine the weathering intensity of the solids ejected from the mud volcanoes. Therefore, CaO related to carbonate minerals was subtracted from the total CaO content to obtain the CaO* content of the silicate fraction [41]. The chemical compositions were also plotted in the A–CN–K ($Al_2O_3 - CaO^* + Na_2O - K_2O$) diagram to identify alteration paths within the mud volcanic ejects [40].

3. Results and Discussion

3.1. Chemical Composition of the Expelled Fluids

The chemical compositions of the fluids expelled from the gryphon-type emissions are reported in Table 1. The fluids extracted from the offshore mud volcanoes in Hamamdagh and Bendovan have pH values of 8.32 and 8.55, which is well within the range of published values since the pH of ~130 mud volcanoes from Azerbaijan varies between 6.51 and 8.84 [16,26,28]. These values are slightly lower compared to the onshore mud volcanoes at Garasu, Khara-Zire and Sangi-Mughan, which exhibit pH values between 8.58 and 9.10. The EC values of all fluids range from 23.3 and 40.8 mS/cm without a systematic geographic trend. The plot of the water compositions in the Piper diagram reveals a Na–Cl-type composition for all fluids (Figure 4), as well as a large overlap with the water chemistries reported for Bahar and Zenbil [4,16]. This suggests that a large fraction of the fluids is sourced from concentrated Caspian seawater due to evaporation.

Table 1. Composition of the fluids expelled from the mud volcanoes in Hamamdagh, Bendovan, Garasu, Khara-Zire and Sangi-Mughan, Azerbaijan. Alkalinity is expressed as HCO_3. Reported EC values correspond to total dissolved solids (TDS) contents of 12.1, 20.4, 11.7, 13.4 and 12.8 g/kg of fluids, respectively. Ion charge balance errors are below 2%. The composition of Caspian seawater is included for comparison (n.a.—not analyzed).

Sample ID	SpC (mS/cm)	T (°C)	pH (−)	Na (mg/L)	K (mg/L)	Mg (mg/L)	Ca (mg/L)	Cl (mg/L)
Garasu	24.1	21.4	8.75	8343	18	71	51	12,702
Sangi-Mughan	40.8	22.0	8.58	13,919	35	109	9	19,756
Hamamdag	23.3	21.6	8.32	8721	20	94	57	12,552
Byandovan	26.8	21.5	8.55	7010	17	82	94	10,192
Khara-Zire	25.5	21.8	9.10	7108	16	12	9	9267

Sample ID	Br (mg/L)	SO_4 (mg/L)	HCO_3 (mg/L)	B (mg/L)	Al (µg/L)	Ba (µg/L)	Cu (µg/L)	Fe (µg/L)
Garasu	48	33	1441	17	146	1063	84	<1
Sangi-Mughan	84	842	2868	13	453	202	117	<1
Hamamdag	78	390	1546	11	155	709	131	83
Byandovan	54	285	1843	19	190	10,808	117	<1
Khara-Zire	47	9	3190	32	61	6372	59	<1

Sample ID	Li (µg/L)	Si (µg/L)	Sr (µg/L)	Zn (µg/L)	As (µg/L)	Na–K (°C)	K–Mg (°C)	SiO_2 (°C)
Garasu	420	2151	8585	642	796	20	57	26
Sangi-Mughan	2271	1893	3085	535	658	25	67	23
Hamamdag	1295	3748	19,104	1023	1141	22	57	41
Byandovan	940	3422	26,338	1023	1420	24	55	38
Khara-Zire	1149	3269	4930	494	618	22	75	37

Accordingly, the fluids are dominated by Na^+ and Cl^- ions, but there is also a considerable range in concentration of the other cations, such as Mg^{2+}, K^+ and Ca^{2+}, and anions, such as hydrogen carbonate HCO_3^-, SO_4^{2-}, Br^- and $B(OH)_3$ (Table 1), which overlap with compositions reported for other mud volcanoes from Azerbaijan [3,4,16,26,28]. The concentrations of K^+, Mg^{2+}, Ca^{2+} and SO_4^{2-} are 3 to 370 times lower compared to Caspian seawater, whereas Na^+, Cl^-, $B(OH)_3$, Br^- and HCO_3^- are enriched by between 2 and 15 times (Table 1). This is due to site-specific mineral dissolution/precipitation reactions, such as smectite illitization, the thermal maturation of organic matter and CH_4 production, dissolution of evaporites exposed in the Maykop Suite shales, redox reactions and weathering processes [11,16,42–47].

All fluids contain a variable, but generally high concentration of dissolved metal ions, such as Al, As, Ba, Cu, Li, Si, Sr and Zn (Table 1), which are similar to mud volcano compositions reported in previous studies [4,11,16,26]. Some of these components are up to several hundred times enriched relative to Caspian seawater. By contrast, the concentration of dissolved Fe is extremely low (Table 1), which is due to the precipitation of iron sulfides, corroborating findings for euhedral pyrite crystals in the mud matrix. Furthermore, this observation is consistent with occurrences of cubic pyrite found in many mud volcanoes across Azerbaijan [48]. These are formed under reducing conditions, as indicated by Eh values of ~30 mud volcanoes in Azerbaijan ranging from −20 to −295 mV [26].

The fluids expelled from the studied mud volcanoes are supersaturated with respect to carbonate minerals, such as aragonite, calcite and dolomite, Fe- and Al-(hydr)oxides (e.g., goethite and gibbsite) and clay minerals, such as Mg-chlorite, illite, Na-montmorillonite and kaolinite (Table 2). Albite, orthoclase and barite are close to saturation or supersaturated with respect to the fluids, whereas anorthite, quartz and evaporite minerals, such as gypsum and halite, are undersaturated (Table 2). No systematic trends in the mineral saturation indices are seen among the different localities.
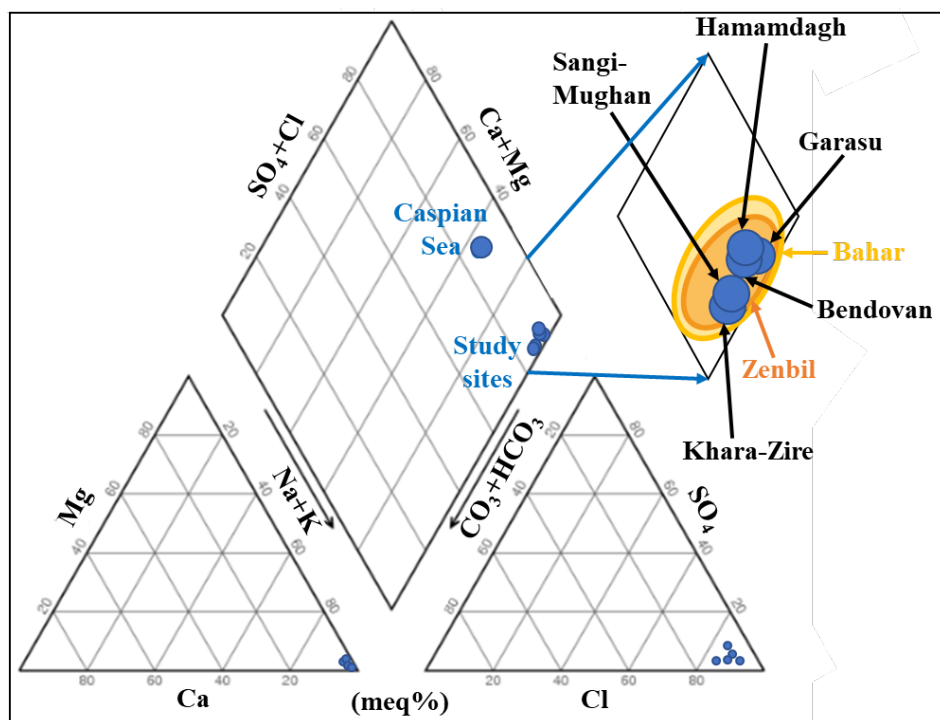
Figure 4. Piper trilinear diagram used for the classification of seep waters collected from the mud volcanoes in Hamamdagh, Bendovan, Garasu, Khara-Zire and Sangi-Mughan, Azerbaijan. Caspian seawater and compositions of fluids ejected in Bahar and Zenbil are included for comparison.

Table 2. Saturation indices of various mineral phases with respect to the fluids expelled from the mud volcanoes in Hamamdagh, Bendovan, Garasu, Khara-Zire and Sangi-Mughan, Azerbaijan. Mineral abbreviations: Ab—albite, An—anorthite, Arg—aragonite, Brt—barite, Cal—calcite, Chl—chlorite, Dol—dolomite, Gbs—gibbsite, Gth—goethite, Gp—gypsum, Hl—halite, Ilt—illite, Kln—kaolinite, Mnt—montmorillonite, Qz, quartz.

Sample ID	Arg (−)	Cal (−)	Dol (−)	Gth (−)	Gbs (−)	Chl (−)	Ilt (−)	Na-Mnt (−)
Garasu	1.3	1.5	4.6	4.7	1.0	8.3	1.5	0.9
Sangi-Mughan	0.6	0.7	4.0	4.7	1.6	8.2	2.7	1.7
Hamamdag	1.0	1.2	4.0	5.7	1.5	6.8	3.7	2.9
Byandovan	1.5	1.7	4.8	4.7	1.3	8.1	3.1	2.4
Khara-Zire	1.0	1.1	3.9	4.6	0.5	6.6	0.5	0.2

Sample ID	Kln (−)	Ab (−)	K-Fsp (−)	Brt (−)	An (−)	Qz (−)	Gp (−)	Hl (−)
Garasu	1.3	0.1	0.3	0.0	−4.5	−0.7	−3.4	−2.8
Sangi-Mughan	2.5	0.6	0.8	0.5	−4.5	−0.7	−2.9	−2.4
Hamamdag	3.2	1.4	1.5	0.8	−3.4	−0.3	−2.2	−2.8
Byandovan	2.6	1.1	1.3	2.0	−3.4	−0.4	−2.1	−3.0
Khara-Zire	0.3	0.0	0.1	0.2	−5.7	−0.6	−4.7	−3.0

3.2. Fluid Origin

The Na^+ and Cl^- concentrations in all sampled fluids are up to 6 times higher than Caspian seawater, but the molar Na/Cl ratio of 1.0 ± 0.1 suggests that the fluids are mainly derived from concentrated Caspian seawater (Figure 4). However, the plot of the Cl–B and Cl–Br relations indicates that the fluids have a mixed origin, which can be described using a two-component mixing model (Figure 5). Type–1 waters have salinities resembling slightly evaporated Caspian seawater, as well as B and Br systematics that are typical of 'low-mineralized' pore fluids, which are sourced from Maykop Suite shales and the Productive

Series strata [4,22,49]. Type–2 waters have a higher degree of mineralization and elevated B and Br concentrations originating from concentrated ancient (Eastern Paratethys-derived) sedimentary pore fluids, which are interpreted as 'high-mineralized' oilfield brines [4,50]. Thus, all fluids are generated via the mixing of modern Caspian seawater and ancient brines sourced from shallow, but not meteoric, to deep reservoir levels. Mazzini et al. [11] and Aliyev et al. [21] argue that the fluids are generated at different depths, including (i) shallow mud chambers within the Productive Series strata (~1 to 5.5 km depth), (ii) moderately deep mud chambers within the Miocene Maykop Suite shales (~5.5 to 9 km depth) and (iii) very deep mud chambers within Eocene-aged strata (up to ~12 km depth). The same conclusions have previously been drawn for the mud and fluid ejects from the mud volcano systems at Bahar and Zenbil [16].
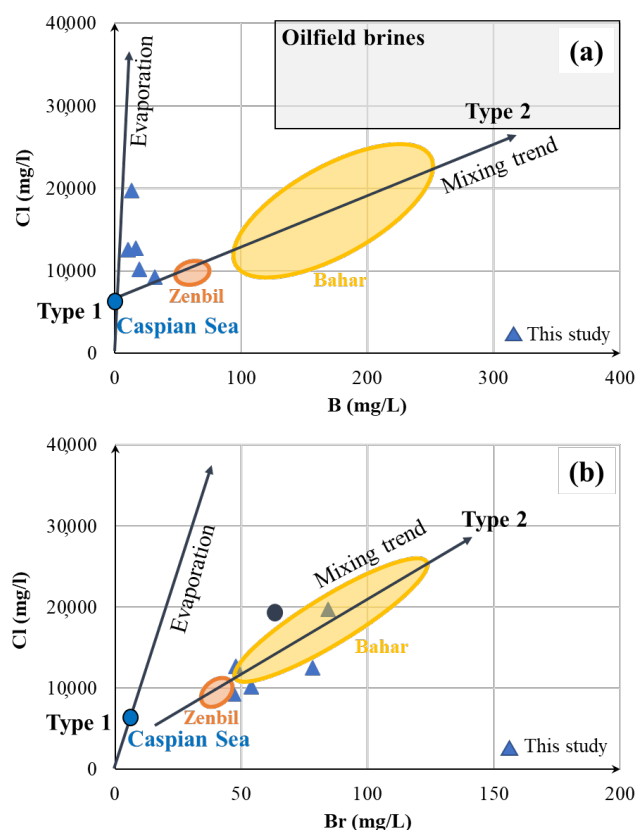

Figure 5. Cross-plots of (**a**) Cl vs. B and (**b**) Cl vs. Br concentrations measured in seep waters. The Cl–B–Br relations of the fluids from the mud volcanoes at Hamamdagh, Bendovan, Garasu, Khara-Zire and Sangi-Mughan (Azerbaijan) reveal a mixed origin, similar to the mud volcanoes at Bahar and Zenbil [16]: Type–1 water = concentrated Caspian seawater; Type–2 water = oilfield brines or ancient sedimentary (highly saline) pore fluids [50]. The ideal evaporation line for Caspian seawater is included for comparison.

The generation temperatures of the fluids range from 20 to 41 °C, with an average of 28 ± 8 °C, as constrained by Na–K and SiO_2 geo-thermometers (Table 1). The applicability of such thermodynamic calculations requires mineral–fluid equilibria, which are barely developed in dynamic mud volcano systems. However, the fluids expelled at Khara-Zire are close to equilibrium with respect to illite and smectite (Table 2), and the calculated mud generation temperatures are comfortably in the range of those calculated for the other localities, suggesting that the obtained generation temperatures of the fluids are correct and realistic within the uncertainty of the geo-thermometers [36]. No systematic trends are seen among the different localities. The K–Mg geo-thermometer yields a higher generation temperature of 55 to 75 °C, averaging 62 ± 9 °C (Table 1), which is too high for the study

sites investigated here. We attribute this to the removal of Mg^{2+} ions from the fluids via the precipitation of dolomite and smectite minerals (see below), thus limiting the reliability of the geo-thermometer. Considering a temperature range from 20 to 41 °C and a geothermal gradient of 10–18 °C/km (average: 15 °C/km) for the South Caspian Sea [5], the formation depth of the fluids varies in the range from ~1.1 to 4.1 km for all localities. Such a shallow origin of the fluids is consistent with previous estimates of mud volcanoes in Bahar and Zenbil, which originate from depths from ~1.8 to 4.2 km [16].

3.3. Mineralogical Composition of Solid Ejects

The mineralogy of the mud samples is identical regarding the liquid, oily and brecciated forms and no geographic differences are observable among the individual localities (Figure 6). The mud is mainly composed of quartz, calcite, calcian dolomite with ~55 mol% $CaCO_3$ and a cation ordering ratio of 0.3–0.5, albite, orthoclase, pyrite and clay minerals, such as illite, chlorite, Na-smectite and kaolinite (Table 3). The Ca excess and low ordering degree of the largely rhombohedral dolomite suggest an authigenic origin of this phase [51], corroborating fluid chemical data (Table 2). Pyrite appears as idiomorphic cubes ranging from millimeters to centimeters in size, also indicating the authigenic origin of this phase [52]. The clay mineral assemblage most likely has a mixed origin and is composed of detrital, platy illite and chlorite, in addition to dominantly authigenic, veil-like to filmy smectite and platelet kaolinite; the latter phases likely represent weathering products of feldspar (Table 2). Sub-rounded quartz, feldspar and likely a fraction of the clay minerals and carbonates are also of detrital origin, being originated from the different sedimentological units the mud is passing through during its ascent. The above described particle forms resemble the prior mineral shapes described by Baldermann et al. [16], which are judged via an SEM (with EDS) analysis during the initial sample inspection, and thus are not shown.

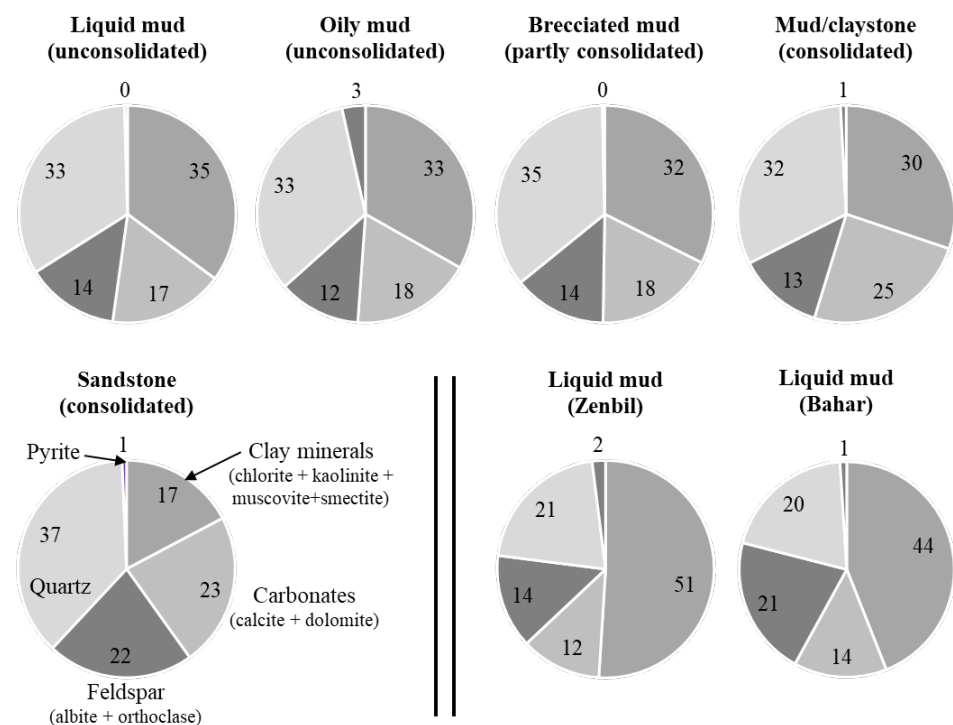**Figure 6.** Comparison of averaged mineralogical compositions obtained for liquid mud (n = 6), oily mud (n = 5), brecciated mud (n = 4), mud/claystones (n = 9) and sandstones (n = 5) collected from the mud volcanoes in Hamamdagh, Bendovan, Garasu, Khara-Zire and Sangi-Mughan, Azerbaijan (cf. Figures 2 and 3 for field impressions). Mud compositions from Bahar and Zenbil are included for comparison (data are from [16]).

Table 3. Mineralogical composition of the mud and sedimentary rocks expelled from the mud volcanoes in Hamamdagh, Bendovan, Garasu, Khara-Zire and Sangi-Mughan, Azerbaijan. The average mineralogical composition of the liquid mud ejects from Bahar (n = 18) and Zenbil (n = 13) is included for comparison (data are from [16]).

Sampling Site	Sample Type	Quartz (wt.%)	Calcite (wt.%)	Dolomite (wt.%)	Albite (wt.%)	Orthoclase (wt.%)
Hamamdagh	Liquid mud	32	13	8	8	2
Hamamdagh	Liquid mud	31	14	1	12	3
Khara-Zire	Liquid mud	40	17	3	11	2
Garasu	Liquid mud	28	14	1	12	2
Sangi-Mughan	Liquid mud	37	14	1	13	2
Sangi-Mughan	Liquid mud	33	14	2	15	2
Hamamdagh	Oily mud	30	16	2	11	2
Bendovan	Oily mud	36	16	1	7	3
Khara-Zire	Oily mud	39	14	1	11	1
Garasu	Oily mud	32	16	1	11	3
Sangi-Mughan	Oily mud	29	22	1	11	2
Hamamdagh	Brecciated mud	35	16	5	13	3
Bendovan	Brecciated mud	29	15	2	9	2
Khara-Zire	Brecciated mud	42	14	2	13	1
Garasu	Brecciated mud	36	15	3	12	2
Hamamdagh	Mud/claystone	29	28	2	14	2
Hamamdagh	Mud/claystone	22	9	35	7	2
Bendovan	Mud/claystone	30	21	1	10	2
Bendovan	Mud/claystone	36	21	1	9	2
Khara-Zire	Mud/claystone	38	12	7	13	1
Garasu	Mud/claystone	32	15	2	12	2
Garasu	Mud/claystone	32	14	7	12	2
Sangi-Mughan	Mud/claystone	33	17	8	11	1
Sangi-Mughan	Mud/claystone	32	14	8	10	3
Bendovan	Sandstone	25	25	1	21	3
Bendovan	Sandstone	31	18	2	21	4
Khara-Zire	Sandstone	55	11	12	14	2
Garasu	Sandstone	39	17	6	20	3
Sangi-Mughan	Sandstone	37	18	4	19	3
Zenbil	Liquid mud	21	10	2	14	1
Bahar	Liquid mud	20	13	1	21	0

Sampling Site	Sample Type	Pyrite (wt.%)	Chlorite (wt.%)	Kaolinite (wt.%)	Illite (wt.%)	Smectite (wt.%)
Hamamdagh	Liquid mud	1	19	1	8	9
Hamamdagh	Liquid mud	0	11	2	17	11
Khara-Zire	Liquid mud	1	8	2	13	4
Garasu	Liquid mud	0	8	2	24	9
Sangi-Mughan	Liquid mud	1	11	2	16	4
Sangi-Mughan	Liquid mud	0	8	2	17	5
Hamamdagh	Oily mud	1	11	1	22	3
Bendovan	Oily mud	12	6	2	9	9
Khara-Zire	Oily mud	1	8	2	17	5
Garasu	Oily mud	1	11	2	18	6
Sangi-Mughan	Oily mud	3	8	2	16	6
Hamamdagh	Brecciated mud	0	8	1	16	3
Bendovan	Brecciated mud	0	13	1	10	19
Khara-Zire	Brecciated mud	1	9	1	10	6
Garasu	Brecciated mud	0	10	1	14	7

Table 3. *Cont.*

Hamamdagh	Mud/claystone	0	13	2	6	4
Hamamdagh	Mud/claystone	0	12	2	9	2
Bendovan	Mud/claystone	0	11	2	17	6
Bendovan	Mud/claystone	0	8	2	14	7
Khara-Zire	Mud/claystone	2	4	1	16	5
Garasu	Mud/claystone	1	10	2	20	5
Garasu	Mud/claystone	1	11	1	15	5
Sangi-Mughan	Mud/claystone	1	9	1	14	5
Sangi-Mughan	Mud/claystone	1	9	2	17	5
Bendovan	Sandstone	1	8	2	5	11
Bendovan	Sandstone	1	5	1	7	9
Khara-Zire	Sandstone	0	1	1	5	0
Garasu	Sandstone	1	7	1	3	2
Sangi-Mughan	Sandstone	1	5	1	7	6
Zenbil	Liquid mud	2	3	8	26	13
Bahar	Liquid mud	1	4	6	22	12

The mud/claystones have slightly lower contents of clay minerals and quartz, a similar feldspar content and a higher carbonate content compared to the mud. The sandstones have the highest contents of quartz and feldspar and moderate carbonate and the lowest clay mineral contents (Figure 6). Compared to the mud compositions reported for Bahar and Zenbil [16], the mud volcanoes investigated in this study have a slightly lower clay mineral content and contain higher amounts of quartz and carbonates (Figure 6).

3.4. Geochemical Composition of Solid Ejects

The geochemical composition of the mud and sedimentary rocks ejected from the mud volcanoes in Hamamdagh, Bendovan, Garasu, Khara-Zire and Sangi-Mughan is summarized in Table 4. The major and minor elemental compositions obtained for all deposit types show minor sample/rock-specific variations, corroborating mineralogical results (Figure 6 and Table 3). Accordingly, the liquid, oily and brecciated mud ejects from all localities have the same chemical composition within analytical uncertainty, averaging 47 ± 5 wt.% SiO_2, 13 ± 1 wt.% Al_2O_3, 16 ± 3 wt.% LOI, 8 ± 1 wt.% CaO, 7 ± 2 wt.% Fe_2O_3, 3 ± 1 wt.% Na_2O, 3 ± 1 wt.% MgO, 2 ± 1 wt.% K_2O and 1 ± 1 wt.% SO_3, with minor TiO_2, MnO and P_2O_5 (<1 wt.%). This composition reflects the abundance of quartz, feldspar, carbonates, clay minerals, pyrite and Ti-bearing phases (most likely rutile) in mud, as previously indicated (Table 3). The mud/claystones exhibit a larger scatter in their CaO, MgO and LOI contents compared to the mud, reflecting the higher proportion of carbonate minerals in this rock type, whereas the sandstones have higher contents of SiO_2 and CaO and lower contents of LOI, Al_2O_3 and Fe_2O_3, which is consistent with increased fractions of quartz and feldspar and reduced amounts of clay minerals in this rock type (Figure 6). As for all eject types, the weak but positive correlation of rubidium (Rb) and vanadium (V) with Al_2O_3 ($R^2 = 0.3$ and 0.4), yttrium (Y; $R^2 = 0.5$ and 0.5), TiO_2 ($R^2 = 0.3$ and 0.5), Ni ($R^2 = 0.3$ and 0.4) and SO_3 ($R^2 = 0.3$ and 0.4) suggests an association with clay minerals, heavy minerals and sulfide minerals, respectively [41]. Barium, Co, Cr, Cu, gallium (Ga), molybdenum (Mo), niobium (Nb), Pb, Sr and Zn are inconspicuous due to either a lack of a correlation with major elements or low concentrations in the samples. However, high Ni/Co ratios (mostly above 5) and low Cu/Zn ratios (mostly below 1) indicate that dysoxic to anoxic conditions prevail within the mud chamber [53], which is consistent with authigenic pyrite found in the mud matrix [48].

Table 4. Geochemical composition of the mud and sedimentary rocks expelled from the mud volcanoes in Hamamdagh, Bendovan, Garasu, Khara-Zire and Sangi-Mughan, Azerbaijan. The average composition of the liquid mud ejects from Bahar and Zenbil is included for comparison (data are from [16]). n.a.—not analyzed. The concentrations of Ga (<20 ppm), Mo (<10 ppm) and Nb (<20 ppm) are always below the detection limit of the XRF analysis.

Sampling Site	Sample Type	Na_2O (wt.%)	MgO (wt.%)	Al_2O_3 (wt.%)	SiO_2 (wt.%)	P_2O_5 (wt.%)	SO_3 (wt.%)	K_2O (wt.%)	CaO (wt.%)
Hamamdagh	Liquid mud	3.0	3.2	13.7	49.8	0.1	0.4	2.3	6.2
Hamamdagh	Liquid mud	2.7	3.0	13.0	44.8	0.1	1.0	2.3	8.1
Khara-Zire	Liquid mud	2.6	3.2	11.7	48.9	0.1	0.3	1.9	10.7
Garasu	Liquid mud	2.9	2.7	13.0	48.9	0.1	0.3	1.9	8.0
Sangi-Mughan	Liquid mud	3.2	2.6	12.5	47.6	0.1	0.8	1.9	7.0
Sangi-Mughan	Liquid mud	3.3	2.7	13.3	48.9	0.1	0.3	2.0	6.7
Hamamdagh	Oily mud	3.3	2.1	13.2	49.9	0.1	0.9	2.0	6.7
Bendovan	Oily mud	2.6	2.5	8.8	32.3	0.4	4.1	1.4	9.7
Khara-Zire	Oily mud	4.0	2.3	13.3	48.5	0.1	0.9	2.0	7.1
Garasu	Oily mud	2.9	2.6	11.8	48.9	0.1	1.4	2.2	9.1
Sangi-Mughan	Oily mud	4.0	2.6	12.2	41.5	0.1	2.5	1.9	8.9
Hamamdagh	Brecciated mud	2.1	3.1	13.5	50.3	0.1	0.4	2.4	7.3
Bendovan	Brecciated mud	2.8	4.0	13.4	43.0	0.1	0.2	2.4	9.5
Khara-Zire	Brecciated mud	2.4	2.4	13.5	50.9	0.1	1.1	2.4	7.4
Garasu	Brecciated mud	2.0	2.6	13.2	50.6	0.1	0.6	2.2	8.4
Hamamdagh	Mud/claystone	3.4	3.3	12.6	47.3	0.1	0.4	1.8	8.0
Hamamdagh	Mud/claystone	1.9	4.4	12.4	42.9	0.1	0.3	2.2	9.1
Bendovan	Mud/claystone	2.6	2.6	14.7	46.0	0.1	0.2	2.3	8.5
Bendovan	Mud/claystone	2.3	2.4	13.6	44.7	0.1	0.1	2.2	8.5
Khara-Zire	Mud/claystone	3.5	2.3	12.0	46.9	0.1	1.4	2.4	7.3
Garasu	Mud/claystone	2.3	2.3	14.1	45.4	0.1	1.3	2.6	8.8
Garasu	Mud/claystone	2.6	2.4	13.2	51.0	0.1	0.1	2.0	6.7
Sangi-Mughan	Mud/claystone	2.5	2.3	13.7	53.9	0.1	0.4	2.0	6.0
Sangi-Mughan	Mud/claystone	1.8	1.4	12.8	63.8	0.1	0.2	2.3	0.5
Bendovan	Sandstone	3.1	2.5	11.8	44.9	0.1	1.6	1.5	13.6
Bendovan	Sandstone	2.9	2.0	12.3	51.2	0.1	1.3	2.1	10.0
Khara-Zire	Sandstone	1.3	1.5	9.4	58.6	0.1	0.5	1.5	12.2
Garasu	Sandstone	3.1	2.6	12.8	55.9	0.1	0.3	1.8	7.0
Sangi-Mughan	Sandstone	3.0	2.2	11.6	53.8	0.1	0.7	1.7	11.1
Zenbil	Liquid mud	2.3	2.3	14.3	52.3	0.1	1.1	1.9	6.4
Bahar	Liquid mud	3.2	2.3	13.2	50.4	0.1	0.6	1.6	8.2

Sampling Site	Sample Type	CaO* (wt.%)	TiO_2 (wt.%)	MnO (wt.%)	Fe_2O_3 (wt.%)	LOI (wt.%)	Ba ppm	Co ppm	Cr ppm
Hamamdagh	Liquid mud	0.2	0.6	0.1	6.0	14.7	455	<20	122
Hamamdagh	Liquid mud	0.1	0.7	0.1	6.4	17.7	454	21	112
Khara-Zire	Liquid mud	0.3	0.6	0.2	5.9	13.9	442	<20	153
Garasu	Liquid mud	0.3	0.6	0.1	5.8	15.5	403	<20	116
Sangi-Mughan	Liquid mud	0.2	0.6	0.1	5.7	18.0	386	<20	128
Sangi-Mughan	Liquid mud	0.4	0.6	0.1	5.8	16.2	753	<20	108
Hamamdagh	Oily mud	0.0	0.6	0.1	5.5	15.4	416	<20	94
Bendovan	Oily mud	0.3	0.6	0.1	13.2	24.2	369	43	118
Khara-Zire	Oily mud	0.5	0.6	0.1	5.6	15.5	480	<20	88
Garasu	Oily mud	0.2	0.7	0.1	6.5	13.7	400	21	177
Sangi-Mughan	Oily mud	0.4	0.9	0.1	7.2	18.0	484	23	105
Hamamdagh	Brecciated mud	0.4	0.6	0.1	6.1	14.1	352	20	157
Bendovan	Brecciated mud	0.4	0.8	0.1	7.4	16.2	390	20	142
Khara-Zire	Brecciated mud	0.3	0.6	0.1	5.7	13.4	396	<20	101
Garasu	Brecciated mud	0.5	0.6	0.1	5.8	13.9	388	<20	113

Table 4. *Cont.*

Hamamdagh	Mud/claystone	0.2	0.6	0.1	6.0	16.6	407	<20	138
Hamamdagh	Mud/claystone	0.2	0.6	0.1	5.9	20.1	265	<20	132
Bendovan	Mud/claystone	0.4	0.6	0.1	5.8	16.6	362	<20	82
Bendovan	Mud/claystone	0.3	0.6	0.1	6.5	18.7	307	21	81
Khara-Zire	Mud/claystone	0.5	0.6	0.1	5.6	17.8	311	<20	96
Garasu	Mud/claystone	0.3	0.6	0.1	5.6	16.8	452	<20	92
Garasu	Mud/claystone	0.3	0.6	0.1	6.1	15.1	403	20	103
Sangi-Mughan	Mud/claystone	0.3	0.7	0.1	5.8	12.6	449	<20	111
Sangi-Mughan	Mud/claystone	0.5	0.7	0.0	5.3	11.1	330	<20	98
Bendovan	Sandstone	0.7	0.7	0.3	5.3	14.6	352	<20	196
Bendovan	Sandstone	0.9	0.5	0.1	4.1	13.5	390	<20	104
Khara-Zire	Sandstone	0.4	0.2	0.1	2.6	12.1	292	<20	21
Garasu	Sandstone	0.2	0.5	0.1	5.0	11.0	378	<20	132
Sangi-Mughan	Sandstone	0.0	0.6	0.1	3.7	11.3	269	<20	363
Zenbil	Liquid mud	0.3	0.6	0.1	5.3	13.3	n.a.	n.a.	n.a.
Bahar	Liquid mud	0.3	0.6	0.1	5.1	14.6	n.a.	n.a.	n.a.

Sampling site	Sample type	Cu ppm	Ni ppm	Rb ppm	Sr ppm	V ppm	Y ppm	Zn ppm	Zr ppm
Hamamdagh	Liquid mud	<20	92	69	415	121	24	29	119
Hamamdagh	Liquid mud	26	101	72	438	125	28	30	126
Khara-Zire	Liquid mud	24	90	56	407	100	24	73	128
Garasu	Liquid mud	24	71	48	368	107	25	33	138
Sangi-Mughan	Liquid mud	21	71	49	362	115	24	29	138
Sangi-Mughan	Liquid mud	20	77	52	654	101	22	30	125
Hamamdagh	Oily mud	<20	52	53	330	108	26	26	143
Bendovan	Oily mud	183	153	42	467	87	37	25	130
Khara-Zire	Oily mud	<20	55	58	676	121	24	29	134
Garasu	Oily mud	71	82	73	392	114	30	82	193
Sangi-Mughan	Oily mud	26	101	40	521	128	33	22	147
Hamamdagh	Brecciated mud	30	95	76	331	122	27	59	134
Bendovan	Brecciated mud	23	100	66	325	124	24	53	137
Khara-Zire	Brecciated mud	24	59	79	362	116	26	42	148
Garasu	Brecciated mud	53	67	71	344	116	25	84	137
Hamamdagh	Mud/claystone	<20	95	43	455	123	23	35	132
Hamamdagh	Mud/claystone	41	111	65	355	134	28	80	113
Bendovan	Mud/claystone	<20	55	76	256	142	26	33	116
Bendovan	Mud/claystone	<20	56	70	267	127	26	46	116
Khara-Zire	Mud/claystone	37	66	68	238	114	24	39	144
Garasu	Mud/claystone	56	100	86	372	110	28	58	135
Garasu	Mud/claystone	32	76	59	254	110	24	58	122
Sangi-Mughan	Mud/claystone	61	70	61	330	107	24	86	132
Sangi-Mughan	Mud/claystone	45	44	90	140	136	36	93	322
Bendovan	Sandstone	<20	66	38	567	100	25	62	139
Bendovan	Sandstone	46	62	51	362	79	<20	61	115
Khara-Zire	Sandstone	<20	<20	45	343	20	23	37	123
Garasu	Sandstone	27	62	46	356	86	20	67	104
Sangi-Mughan	Sandstone	26	51	42	103	76	<20	55	120
Zenbil	Liquid mud	n.a.	n.a.	n.a.	n.a.	n.a.	n.a.	n.a.	n.a.
Bahar	Liquid mud	n.a.	n.a.	n.a.	n.a.	n.a.	n.a.	n.a.	n.a.

The plot of the chemical data in the A–CN–K diagram illustrates that all sample types fall slightly above the compositional range of Average Proterozoic Shale (APS) and Post-Archean Australian Shale (PAAS), but generally follow the predicted weathering trend for Upper Continental Crust (UCC) rocks (Figure 7). There is also a considerable overlap with the mud compositions reported in Bahar and Zenbil [16], although the mud ejects from all studied localities have slightly lower contents of Al_2O_3 and SiO_2, which we attribute to a lower clay mineral content (Figure 6). No evidence for sorting (i.e., shift towards the A pole) and K-metasomatism (i.e., shift towards the K pole) is seen. The CIA values are very high compared to basalt (30–45), granite/granodiorite (45–55) and feldspar (50), respectively, i.e., they vary in a range from 66 to 74 for all sample types studied among the different localities (Figure 7). This feature suggests that the solid ejects experience post-depositional

alterations due to fluid–rock–gas reactions and mud diagenesis. Previous studies have shown that these weathering processes can reach a depth of 10 km [5,21,54].
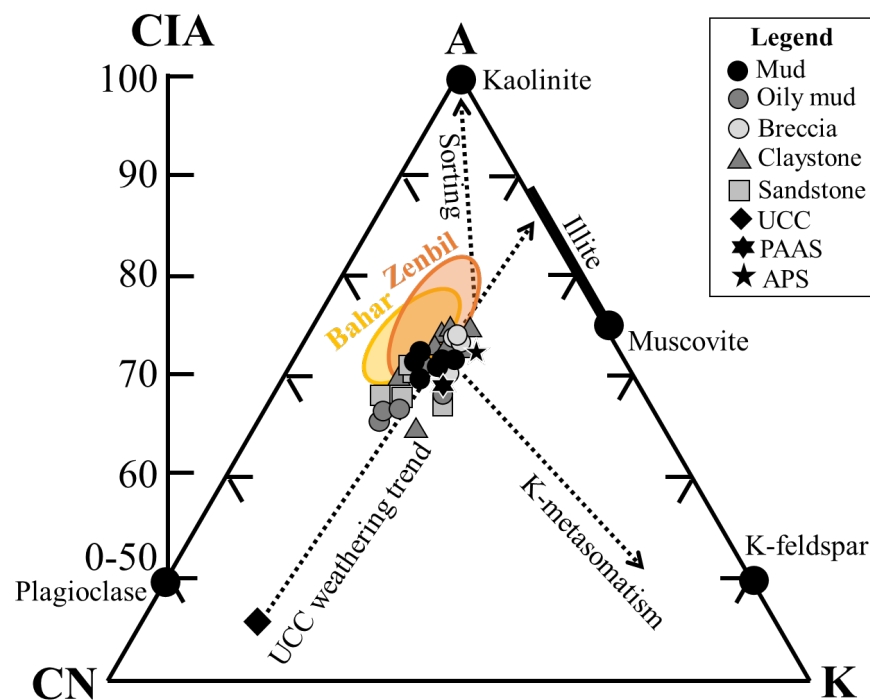

Figure 7. Chemical compositions of the mud and sedimentary rocks ejected from the mud volcanoes in Hamamdagh, Bendovan, Garasu, Khara-Zire and Sangi-Mughan, Azerbaijan, plotted in the A–CN–K diagram. The compositions of the Upper Continental Crust (UCC), Post-Archean Australian Shale (PAAS) and Average Proterozoic Shale (APS) are included for comparison. CIA = Chemical Index of Alteration (A < 50 is not shown).

3.5. Origin of Solid Ejects

Petrographic, mineralogical and chemical comparisons of all solid ejects from the mud volcanoes at Hamamdagh, Bendovan, Garasu, Khara-Zire and Sangi-Mughan with lithofacies description and the interpretation of several Productive Series outcrops from the South Caspian Basin by Hinds et al. [25] suggests that the majority of the mud, mud/claystones and sandstones are sourced from Pleistocene–Pliocene-aged intervals located in ~1 to 4 km depth, corroborating the calculated fluid generation temperatures (~30 ± 10 °C) and depths (~1–4 km depth). Moreover, Upper Productive Series strata found in several outcrops across the Absheron Peninsula (Azerbaijan), such as sandstones and silt- to mudstones, have mineralogical compositions that resemble those of the lithogenic fragments described in this study [55]. For example, the fined-grained Yasamal Valley sedimentary rocks mainly comprise quartz (15–40 wt.%), feldspar (10–20 wt.%), calcite (10–25 wt.%) and clay minerals (20–60 wt.%), which mineralogically overlap with the mud and mudstones ejected from the five new mud volcanoes (Table 3). Although the sandstone lithologies cropping up in the Yasamal Valley have higher quartz contents (up to 70 wt.%), on average, they are partially pervasively cemented with calcite and minor dolomite (30–40 wt.%), consistent with our petrographic observations made for coarse-grained lithologies [55].

The expelled sandstones and mud/claystones have been interpreted as channelized and sheetflood fluvial deposits and short-lived alluvial plane and lacustrine deposits of a regional Caspian lake, respectively [25,56]. Aliyev et al. [15] argue that these sedimentary rocks are sourced from Jurassic- and Cretaceous-aged, mafic-intermediate, volcanic-to-clastic deposits exposed on the southern slope of the Greater Caucasus (Tufan and Vandam uplifts), as well as from Paleogene- to Miocene-aged, sea and coastal volcanic products and shales of the Gobustan and Absheron peninsulas. The Productive Series sediments of

the South Caspian Basin (especially the sand facies) are further sourced from the Russian platform drained by the paleo-Volga river [56]. Moreover, the integration of the drainage systems (paleo-Volga, paleo-Kura and paleo-Amu Darya) resulted in the extensive supply of sediments from the Russian Platform, Caucasus and Pamir/Kopet-Dagh Mountains, which were deposited as fluvio-lacustrine facies in pre-existing structural depressions of the South Caspian Basin.

The Productive Series strata were deposited during the most dramatic sea level low-stand tract that the Caspian Sea has ever experienced. The extremely high fluvio-deltaic input of the paleo-Volga river also resulted in high depositional rates of the Productive Series sediments of greater than 1.5 km/million years, which ash lasted for at least the last 5 million years [57], producing a ~7–8 km thick sedimentary sequence within the South Caspian Basin that rapidly underwent subsidence and burial diagenesis [58]. Simultaneously, the smaller paleo-Kura and paleo-Amu Darya rivers likely also contributed to the development of the Productive Series strata as well. Rapid burial, post-depositional alterations due to strong fluid–rock–gas reactions and mud diagenesis in a compressive tectonic setting of the South Caspian Basin finally resulted in mud diapirism [16], which expresses in the development of today's landscape of large areas in eastern Azerbaijan and in the formation of new mud volcanic islands within the shallow water regions in the Caspian Sea (Figure 1). Thus, fluid and solid sources for mud volcanic activities are mainly provided by mud chambers to be situated in the Productive Series strata (1 to 5.5 km depth), although a minor contribution from deeper reservoirs (e.g., Maykop Suite shales ranging from 5.5 to 9 km depth and Eocene rocks up to 12 km depth) is likely [21,58,59]. The highly complex architecture of the South Caspian Basin and the mixed origin of the mud volcanic ejects explain the observed chemical and mineralogical compositions of the fluids and mud.

4. Conclusions

The geochemical and mineralogical compositions of fluid, mud and rock ejects from five new mud volcanoes located in continental Azerbaijan (Hamamdagh and Bendovan) and in the Caspian Sea (Garasu, Khara-Zire and Sangi-Mughan) were investigated and compared with published compositions of mud and fluids expelled at the mud volcano systems at Bahar (Shamakhi-Gobustan region) and Zenbil (Caspian Sea, Baku Archipelago). The expelled fluids have a Na-Cl composition and are generated via the mixing of evaporated Caspian seawater, shallow 'low-mineralized' pore fluids and deep-seated 'high-mineralized' brines. The fluids contain elevated concentrations of dissolved metal ions (Al, As, Ba, Cu, Li, Si, Sr and Zn: ~60–26,300 µg/L) due to smectite illitization, hydrocarbon maturation and methane production, redox reactions and complex dissolution–precipitation processes involving clay minerals and carbonates. The fluids are generated in Productive Series strata in ~1 to 4 km depth, similar to the mud volcanoes at Bahar and Zenbil (~2 to 4 km depth). The mud is composed of quartz, albite, orthoclase, illite, chlorite, calcite, calcian dolomite, pyrite, Na-smectite and kaolinite. All study sites show lower contents of clay minerals, but higher amounts of quartz and carbonates compared to mud compositions reported in Bahar and Zenbil. However, there is a large mineralogical and chemical overlap of all mud compositions. Chemical element ratios (Ni/Co and Cu/Zn) suggest that the mud forms under anaerobic conditions. The ejected mud, mud/claystones and sandstones are sourced from giant mud chambers located in Productive Series strata, partially fed by deeper reservoirs (Maykop Suite shales and Eocene rocks).

References

1. Kopf, A.J. Significance of mud volcanism. *Rev. Geophys.* **2002**, *40*, 2–52. [CrossRef]
2. Chao, H.-C.; You, C.-F.; Lin, I.-T.; Liu, H.-C.; Chung, L.-H.; Huang, C.-C.; Chung, C.-H. Two-End-Member Mixing in the Fluids Emitted from Mud Volcano Lei-Gong-Huo, Eastern Taiwan: Evidence from Sr Isotopes. *Front. Earth Sci.* **2022**, *9*, 750436. [CrossRef]
3. Aliyev, A.A.; Guliyev, I.S.; Belov, S. Catalogue of Recorded Eruptions of Mud Volcanoes of Azerbaijan for Period of Years 1810–2001. In *Baku Institute of Geology of the Azerbaijan National Academy of Sciences*; Nafta Press: Baku, Azerbaijan, 2002; pp. 1–88.
4. Planke, S.; Svensen, H.; Hovland, M.; Banks, D.A.; Jamtveit, B. Mud and fluid migration in active mud volcanoes in Azerbaijan. *Geo-Mar. Lett.* **2003**, *23*, 258–268. [CrossRef]
5. Bonini, M.; Tassi, F.; Feyzullayev, A.A.; Aliyev, C.S.; Capecchiacci, F.; Minissale, A. Deep gases discharged from mud volcanoes of Azerbaijan: New geochemical evidence. *Mar. Petrol. Geol.* **2013**, *43*, 450–463. [CrossRef]
6. Kokh, S.N.; Sokol, E.V. Combustion Metamorphism in Mud Volcanic Events: A Case Study of the 6 May 2000 Fire Eruption of Karabetova Gora Mud Volcano. *Minerals* **2023**, *13*, 355. [CrossRef]
7. Jones, R.W.; Simmons, M.D. A review of the stratigraphy of eastern Paratethys (Oligocene–Holocene), with particular emphasis on the Black Sea. In *Regional and Petroleum Geology of the Black Sea and Surrounding Regions*; Robinson, A., Ed.; AAPG Memoir: Tulsa, OK, USA, 1997; Volume 68, pp. 39–52.
8. Etiope, G.; Klusman, R.W. Geologic emissions of methane to the atmosphere. *Chemosphere* **2002**, *49*, 779–791. [CrossRef]
9. Charlou, J.L.; Donval, J.P.; Zitter, T.; Roy, N.; Jean-Baptiste, P.; Foucher, J.P.; Woodside, J. Evidence of methane venting and geochemistry of brines on mud volcanoes of the eastern Mediterranean Sea. *Deep-Sea Res. Pt. I* **2003**, *50*, 941–958. [CrossRef]
10. Etiope, G.; Milkov, A. A new estimate of global methane flux from onshore and shallow submarine mud volcanoes to the atmosphere. *Environ. Geol.* **2004**, *46*, 997–1002. [CrossRef]
11. Mazzini, A.; Svensen, H.; Planke, S.; Guliyev, I.; Akhmanov, G.G.; Fallik, T.; Banks, D. When mud volcanoes sleep: Insight from seep geochemistry at the Dashgil mud volcano, Azerbaijan. *Mar. Petrol. Geol.* **2009**, *26*, 1704–1715. [CrossRef]
12. Deville, E.; Guerlais, S.-H.; Lallemant, S.; Schneider, F. Fluid dynamics and subsurface sediment mobilization processes: An overview from Southeast Caribbean. *Basin Res.* **2010**, *22*, 361–379. [CrossRef]
13. Bonini, M. Mud volcanoes: Indicators of stress orientation and tectonic controls. *Earth-Sci. Rev.* **2012**, *115*, 121–152. [CrossRef]
14. Baloglanov, E.E.; Abbasov, O.R.; Akhundov, R.V. Mud volcanoes of the world: Classifications, activities and environmental hazard (informational-analytical review). *Geogr. Sci.* **2018**, *5*, 12–26.
15. Aliyev, A.A.; Abbasov, O.R.; Agayev, A.M. Mineralogy and geochemistry of oil shale in Azerbaijan: Classification, paleo-weathering and maturity features. *Visnyk V. N. Karazin Kharkiv Natl. Univ. Ser. Geology. Geography. Ecol.* **2019**, *50*, 11–26.
16. Baldermann, A.; Abbasov, O.R.; Bayramova, A.; Abdullayev, E.; Dietzel, M. New insights into fluid-rock interaction mechanisms at mud volcanoes: Implications for fluid origin and mud provenance at Bahar and Zenbil (Azerbaijan). *Chem. Geol.* **2020**, *537*, 119479. [CrossRef]
17. Milkov, A.V. Worldwide distribution of submarine mud volcanoes and associated gas hydrates. *Mar. Geol.* **2000**, *167*, 29–42. [CrossRef]
18. Dimitrov, L.I. Mud volcanoes—The most important pathway for degassing deeply buried sediments. *Earth Sci. Rev.* **2002**, *59*, 49–76. [CrossRef]
19. Jakubov, A.A.; Ali-Zade, A.A.; Zeinalov, M.M. *Mud Volcanoes of the Azerbaijan SSR*; Atlas; Azerbaijan Academy of Sciences: Baku, Azerbaijan, 1971; pp. 1–258. (In Russian)
20. Devlin, W.; Cogswell, J.; Gaskins, G.; Isaksen, G.; Pitcher, D.; Puls, D.; Stanley, K.; Wall, G. South Caspian Basin: Young, cool, and full of promise. *GSA Today* **1999**, *9*, 1–9.
21. Aliyev, A.A.; Guliyev, I.S.; Dadashev, F.G.; Rahmanov, R.R. Atlas of mud volcanoes in the world. In *Baku Institute of Geology and Geophysics of the Azerbaijan National Academy of Sciences*; Nafta Press: Baku, Azerbaijan, 2015; pp. 1–361.
22. Guliyev, I.S.; Feizullayev, A.A. Geochemistry of hydrocarbon seepages in Azerbaijan. In *Hydrocarbon Migration and Its Near Surface Expression*; Schumacher, D., Abrams, M.A., Eds.; AAPG Memoir: Tulsa, OK, USA, 1996; Volume 66, pp. 63–70.
23. Abbasov, O.R. Oil Shale of Azerbaijan: Geology, Geochemistry and Probable Reserves. *Int. J. Res. Stud. Sci. Eng. Technol.* **2015**, *2*, 31–37.

24. Fowler, S.R.; Mildenhall, J.; Zalova, S.; Riley, G.; Elsley, G.; Desplanques, A.; Guliyev, F. Mud volcanoes and structural development on Shah Deniz. *J. Petrol. Sci. Eng.* **2000**, *28*, 189–206. [CrossRef]

25. Hinds, D.J.; Aliyeva, E.; Allen, M.B.; Davies, C.E.; Kroonenberg, S.B.; Simmons, M.D.; Vincent, S.J. Sedimentation in a discharge dominated fluvial-lacustrine system: The Neogene Productive Series of the South Caspian Basin, Azerbaijan. *Mar. Pet. Geol.* **2004**, *21*, 613–638. [CrossRef]

26. Lavrushin, V.Y.; Guliev, I.S.; Kikvadze, O.E.; Aliev, A.A.; Pokrovsky, B.G.; Polyak, B.G. Waters from Mud Volcanoes of Azerbaijan: Isotopic–Geochemical Properties and Generation Environments. *Lithol. Miner. Resour.* **2015**, *50*, 1–25. [CrossRef]

27. Bujakaite, M.I.; Lavrushin, V.Y.; Pokrovsky, B.G. Strontium Isotope Composition of Mud Volcanic Waters in Azerbaijan. *Lithol. Miner. Resour.* **2019**, *54*, 351–361. [CrossRef]

28. Kikvadze, O.E.; Lavrushin, V.Y.; Polyak, B.G. Chemical geothermometry: Application to mud volcanic waters of the Caucasus region. *Front. Earth Sci.* **2020**, *14*, 738–757. [CrossRef]

29. Eichinger, S.; Boch, R.; Leis, A.; Baldermann, A.; Domberger, G.; Schwab, C.; Dietzel, M. Green inhibitors reduce unwanted calcium carbonate precipitation: Implications for technical settings. *Wat. Res.* **2022**, *208*, 117850. [CrossRef]

30. Boch, R.; Dietzel, M.; Reichl, P.; Leis, A.; Baldermann, A.; Mittermayr, F.; Pölt, P. Rapid ikaite ($CaCO_3 \cdot 6H_2O$) crystallization in a man-made river bed: Hydrogeochemical monitoring of a rarely documented mineral formation. *Appl. Geochem.* **2015**, *63*, 366–379. [CrossRef]

31. Baldermann, A.; Abdullayev, E.; Taghiyeva, Y.; Alasgarov, A.; Javad-Zada, Z. Sediment petrography, mineralogy and geochemistry of the Miocene Islam Dağ Section (Eastern Azerbaijan): Implications for the evolution of sediment provenance, palaeo-environment and (post-)depositional alteration patterns. *Sedimentology* **2020**, *67*, 152–172. [CrossRef]

32. Parkhurst, D.L.; Appelo, C.A.J. Description of input and examples for PHREEQC version 3-A computer program for speciation, batch-reaction, one-dimensional transport, and inverse geochemical calculations. In *US Geological Survey Techniques and Methods*; U.S. Geological Survey: Denver, CO, USA, 2013; Volume 6, pp. 1–497.

33. Fournier, R.O. A Revised Equation for the Na/K Geothermometer. *Geotherm. Resour. Counc. Trans.* **1979**, *3*, 221–224.

34. Giggenbach, W.F. Geothermal Solute Equilibria. Derivation of the Na-K-Mg-Ca Geoindicators. *Geochim. Cosmochim. Acta* **1988**, *52*, 2749–2765. [CrossRef]

35. Fournier, R.O. Chemical Geothermometers and Mixing Models for Geothermal Systems. *Geothermics* **1977**, *5*, 41–50. [CrossRef]

36. Wishart, D.B.N. Comparison of silica and cation geothermometers of bath hot springs, Jamaica WI. In Proceedings of the World Geothermal Congress, Melbourne, Australia, 19–24 April 2015; pp. 1–13.

37. Richoz, S.; Baldermann, A.; Frauwallner, A.; Harzhauser, M.; Daxner-Höck, G.; Klammer, D.; Piller, W.E. Geochemistry and mineralogy of the Oligo-Miocene sediments of the Valley of Lakes, Mongolia. *Paleobiodivers. Paleoenviron.* **2017**, *97*, 233–258. [CrossRef]

38. Han, S.; Löhr, S.C.; Abbott, A.N.; Baldermann, A.; Farkaš, J.; McMahan, W.; Milliken, K.L.; Rafiei, M.; Wheeler, C.; Owen, M. Earth system science applications of next-generation SEM-EDS automated mineral mapping. *Front. Earth Sci.* **2022**, *10*, 956912. [CrossRef]

39. Baldermann, A.; Wasser, O.; Abdullayev, E.; Bernasconi, S.; Löhr, S.; Wemmer, K.; Piller, W.E.; Rudmin, M.; Richoz, S. Palaeoenvironmental evolution of Central Asia during the Cenozoic: New insights from the continental sedimentary archive of the Valley of Lakes (Mongolia). *Clim. Past* **2021**, *17*, 1955–1972. [CrossRef]

40. Nesbitt, H.W.; Young, G.M. Prediction of some weathering trends of plutonic and volcanic rocks based on thermodynamic and kinetic considerations. *Geochim. Cosmochim. Acta* **1984**, *48*, 1523–1534. [CrossRef]

41. Abdullayev, E.; Baldermann, A.; Warr, L.N.; Grathoff, G.; Taghiyeva, Y. New constraints on the palaeo-environmental conditions of the Eastern Paratethys: Implications from the Miocene Diatom Suite (Azerbaijan). *Sed. Geol.* **2021**, *411*, 105794. [CrossRef]

42. Linnikov, O.D.; Podbereznyi, V.L.; Anokhina, E.A.; Guseva, O.V. Efficiency of two scale prevention methods for desalting Caspian Seawater. *Desalination* **1993**, *89*, 311–323. [CrossRef]

43. Kopf, A.; Deyhle, A. Back to the roots: Boron geochemistry of mud volcanoes and its implications for mobilization depth and global B cycling. *Chem. Geol.* **2002**, *192*, 195–210. [CrossRef]

44. James, R.H.; Allen, D.E.; Seyfried, W.E. An experimental study of alteration of oceanic crust and terrigenous sediments at moderate temperatures (51 to 350 °C): Insights as to chemical processes in near-shore ridge-flank hydrothermal systems. *Geochim. Cosmochim. Acta* **2003**, *67*, 681–691. [CrossRef]

45. Li, N.; Huang, H.; Chen, D. Fluid sources and chemical processes inferred from geochemistry of pore fluids and sediments of mud volcanoes in the southern margin of the Junggar Basin, Xinjiang, northwestern China. *Appl. Geochem.* **2014**, *46*, 1–9. [CrossRef]

46. Carvalho, L.; Monteiro, R.; Figueira, P.; Mieiro, C.; Almeida, J.; Pereira, E.; Magalhães, V.; Pinheiro, L.; Vale, C. Vertical distribution of major, minor and trace elements in sediments from mud volcanoes of the Gulf of Cadiz: Evidence of Cd, As and Ba fronts in upper layers. *Deep-Sea Res. Pt. I* **2018**, *131*, 133–143. [CrossRef]

47. Sokol, E.V.; Kokh, S.N.; Kozmenko, O.A.; Lavrushin, V.Y.; Belogub, E.V.; Khvorov, P.V.; Kikvadze, O.E. Boron in an Onshore Mud Volcanic Environment: Case Study from the Kerch Peninsula, the Caucasus Continental Collision Zone. *Chem. Geol.* **2019**, *525*, 58–81. [CrossRef]

48. Aliev, A.A.; Lavrushin, V.Y.; Kokh, S.V.; Sokol, E.V.; Petrov, O.L. Isotopic Composition of Pyritic Sulfur from the Mud Volcanic Ejecta in Azerbaijan. *Lithol. Miner. Resour.* **2017**, *52*, 358–368. [CrossRef]

49. Guliyev, I.S.; Huseynov, D.A.; Feizullayev, A.A. Fluids of mud volcanoes in the Southern Caspian sedimentary basin: Geochemistry and sources in light of new data on the carbon, hydrogen, and oxygen isotopic compositions. *Geochem. Int.* **2004**, *42*, 688–695.
50. Collins, A.G. *Geochemistry of Oilfield Waters*; Elsevier: New York, NY, USA, 1975; pp. 1–495.
51. Kell-Duivestein, I.J.; Baldermann, A.; Mavromatis, V.; Dietzel, M. Controls of temperature, alkalinity and calcium carbonate reactant on the evolution of dolomite and magnesite stoichiometry and dolomite cation ordering degree—An experimental approach. *Chem. Geol.* **2019**, *529*, 119292. [CrossRef]
52. Raiswell, R.; Canfield, D.E. The Iron Biogeochemical Cycle Past and Present. *Geochem. Perspect.* **2012**, *1*, 1–232. [CrossRef]
53. Hallberg, R.O. A Geochemical Method for Investigation of Palaeoredox Conditions in Sediments. *Ambio Spec. Rep.* **1976**, *4*, 139–147.
54. Inan, S.; Yalcin, M.N.; Guliyev, I.S.; Kuliev, K.; Feizullayev, A.A. Deep petroleum occurrences in the lower Kura depression, south Caspian Basin, Azerbaijan: An organic geochemical and basin modelling study. *Mar. Petroleum Geol.* **1997**, *14*, 731–762. [CrossRef]
55. Shahtakhtinskiy, A.; Khan, S. 3D stratigraphic mapping and reservoir architecture of the Balakhany Suite, Upper Productive Series, using UAV photogrammetry: Yasamal Valley, Azerbaijan. *Mar. Petrol. Geol.* **2022**, *145*, 105911. [CrossRef]
56. Kroonenberg, S.B.; Alekseevski, N.I.; Aliyeva, E.; Allen, M.B.; Aybulatov, D.N.; Baba-Zadeh, A.; Badyukova, E.N.; Davies, C.E.; Hinds, D.J.; Hoogendoorn, R.M.; et al. Two Deltas, Two Basins, One River, One Sea: The Modern Volga Delta as an Analogue of the Neogene Productive Series, South Caspian Basin. In *River Deltas-Concepts, Models, and Examples*; Giosan, L., Ed.; SEPM Society for Sedimentary Geology: Broken Arrow, OK, USA, 2005. [CrossRef]
57. Knapp, J.H.; Knapp, C.C.D.; Connor, J.A.; McBride, J.H.; Simmons, M.D. Deep seismic exploration of the South Caspian Basin: Lithosphere-scale imaging of the world's deepest basin. In *Oil and Gas of the Greater Caspian Area*; Yilmaz, P.O., Isaksen, G.H., Eds.; AAPG Studies in Geology; American Association of Petroleum Geologists: Tulsa, OK, USA, 2007. [CrossRef]
58. Adullayev, E.; Leroy, S. Provenance of clay minerals in the sediments from the Pliocene Productive Series, western South Caspian Basin. *Mar. Petrol. Geol.* **2016**, *73*, 517–527. [CrossRef]
59. Feyzullayev, A.A. Mud volcanoes in the South Caspian basin: Nature and estimated depth of its products. *Nat. Sci.* **2012**, *4*, 445–453. [CrossRef]